Fluctuation and Noise Letters
Vol. 13, No. 4 (2014) 1450025 (23 pages)

DOI: 10.1142/S0219477514500254

World Scientific
www.worldscientific.com

Information-Theoretic Modeling of Trichromacy Coding of Light Spectrum

Landry Benoit* and Étienne Belin†

Laboratoire Angevin de Recherche en Ingénierie des Systèmes (*LARIS*)
Université d'Angers, 62 Avenue Notre Dame du Lac, 49000 Angers, France
**landry.benoit@univ-angers.fr*
†*etienne.belin@univ-angers.fr*

David Rousseau

Université de Lyon, CREATIS, CNRS UMR 5220, INSERM U1044
Université Lyon 1, INSA-Lyon, 69621 Villeurbanne, France
david.rousseau@univ-lyon1.fr

François Chapeau-Blondeau

Laboratoire Angevin de Recherche en Ingénierie des Systèmes (*LARIS*)
Université d'Angers, 62 Avenue Notre Dame du Lac, 49000 Angers, France
chapeau@univ-angers.fr

Received 11 March 2014
Accepted 26 June 2014
Published 10 July 2014

Communicated by Stefania Residori

Trichromacy is the representation of a light spectrum by three scalar coordinates. Such representation is universally implemented by the human visual system and by RGB (Red Green Blue) cameras. We propose here an informational model for trichromacy. Based on a statistical analysis of the dynamics of individual photons, the model demonstrates a possibility for describing trichromacy as an information channel, for which the input–output mutual information can be computed to serve as a measure of performance. The capabilities and significance of the informational model are illustrated and motivated in various situations. The model especially enables an assessment of the influence of the spectral sensitivities of the three types of photodetectors realizing the trichromatic representation. It provides a criterion to optimize possibly adjustable parameters of the spectral sensitivities such as their center wavelength, spectral width or magnitude. The model shows, for instance, the usefulness of some overlap with smooth graded spectral sensitivities, as observed for instance in the human retina. The approach also, starting from hyperspectral images with high spectral resolution measured in the laboratory, can be used to devise low-cost trichromatic imaging systems optimized for observation of specific spectral signatures. This is illustrated with an example from plant science, and demonstrates a potential of application especially to life sciences. The approach particularizes connections between physics, biophysics and information theory.

Keywords: Information theory; photon statistics; light spectrum; trichromacy; color; vision.

1. Introduction

Information-theoretic concepts show more and more impact at the frontier with physics [1–4], including biophysics [5, 6]. At this frontier some important issues lie in the ways of quantifying information, in the resulting operational significance in the physical world, in the connections of information with its physical supports and with physical laws. For a contribution at this interface of physics and information theory, we consider here the domain of optics, light signal and imaging [7–9], and demonstrate the possibility of constructing an information-theoretic description of the process of trichromacy.

We consider a light spectrum denoted $S(\lambda)$ and supported by the domain of wavelength $\lambda \in [\lambda_{\min}, \lambda_{\max}]$. A typical reference for $S(\lambda)$ is the spectrum of visible light radiated by a colored object in the visible range $\lambda \in [\lambda_{\min} = 400\,\text{nm}, \lambda_{\max} = 700\,\text{nm}]$. High-resolution spectrometers or hyperspectral cameras are capable of accurately measuring such a light spectrum. However, devices exist with a much more reduced spectral resolution, such as RGB cameras or the human retina, which represent a continuous spectrum $S(\lambda)$ over $\lambda \in [\lambda_{\min}, \lambda_{\max}]$, by a few scalar values. This is the case with trichromacy coding of a light spectrum, which replaces the continuous spectrum $S(\lambda)$ by three scalar values $(\text{R}, \text{G}, \text{B})$.

One can intuitively expect some significant reduction of information when a continuous spectrum $S(\lambda)$ is replaced by three scalars $(\text{R}, \text{G}, \text{B})$. Common RGB cameras and the human retina implement this type of representation. Such systems exploit light spectra to produce color images, and their (reduced) spectral representation is targeting toward a sufficiently efficient discrimination of objects of the environment in the imaged scene, rather than toward a complete restitution of their radiated spectra. Color images produced in this way are usually valuable for their informational content. It is therefore specially relevant to develop an *informational* analysis of the representation of a continuous spectrum $S(\lambda)$ by three scalar values $(\text{R}, \text{G}, \text{B})$. An informational approach to trichromacy is specially appealing because trichromacy, as a natural process implemented by visual processing, involves sensory systems refined and optimized over biological evolution and associated with high performance for information processing by vision [10, 11]. We propose such an approach here, with the elaboration of an informational model for trichromacy and the study of its properties.

Informational contents for physical signals can be defined and quantified in a powerful way by means of statistical information theory, as pioneered by Shannon [12, 13]. If one wants to apply such an approach to light spectra, one needs to setup a statistical description in this area. Light spectra are not immediately given as statistical objects, a fortiori endowed with a univocal statistical significance. Several approaches can be envisaged to describe light spectra in a statistical framework, and these can be understood through an analogy with images. Images in the same way are not immediately given as statistical objects. To formalize images in a statistical framework, an approach is to consider an image as giving access

to one or several realizations of a statistical process. An image can be identified with one realization drawn from a statistical ensemble of images; or alternatively, each pixel of an image can be identified with one realization of a statistical process. Such realizations can be combined in order to obtain an estimation of relevant probability distributions of the underlying statistical process. This is essentially this type of approach which has been exploited so far for informational descriptions of light spectra in imagery [14–18]. This approach relies on, and reflects, its basic hypothesis: what is observed are realizations; and accordingly it critically depends on the number of accessible realizations for estimating the underlying probability distributions, which often is a limiting factor in a statistical description.

Another, distinct, approach consists in considering an image, not as a realization from a statistical process, but as a probability distribution in itself. This type of approach has been introduced in imaging [19–22], and shown fruitful, for informational studies such as the application of the principle of maximum entropy. The basis of this approach receives justification from the law of large numbers, when very large numbers of photons are involved in the process of image formation. Image intensities and their spatial distributions are related to populations of photons and their relative proportions interpretable as probability distributions. This view of light intensities as probability distributions is also consistent with the specifications of quantum optics for the photon [23]. In this way, this approach relies on, and reflects, a distinct basic hypothesis: what is observed are probability distributions. Accordingly, it is not affected by limiting issues concerning the number of accessible realizations, and it is able to derive from one observation an informational interpretation based on statistical information theory.

It is this type of approach, we will apply here to light spectra, in order to derive an information-theoretic assessment of trichromacy. A light spectrum will be considered as a probability distribution related to the dynamics of individual photons. On this basis, we demonstrate the possibility to construct an informational model for the trichromatic (or multichromatic) coding of light spectra. We then analyze the properties of the model in different situations. This serves two main purposes, first to appreciate and assess the capabilities and significance of the model and its assumptions as an informational description, and second to exploit the model for a quantitative characterization of trichromacy and optimization of its performance.

Some other informational approaches to trichromacy, based on statistical information theory as we do here, have previously been proposed. The approach of [24] starts from three primitive components R, G and B, and studies how the visual system can combine or transform them efficiently, especially through color opponency. An efficient transformation is obtained through decorrelation of the three R, G, B components, by a Karhunen–Loeve expansion or principal component analysis, as also advocated in [25]. Information theory is invoked to motivate a decorrelating transformation as achieving optimal information compaction (energy compaction) as explained in [24], although some other informational aspects remain invariant

since the transformation is invertible. Also, the approach of [24] depends on the assumed statistics over an ensemble of input light spectra [24, 26]. By contrast here, our informational approach to trichromacy will operate at a lower level, essentially for assessing the impact of the spectral sensitivities of the photodetectors implementing the trichromatic (R, G, B) representation, rather than for assessing higher-level operations performed by the visual system on the three components R, G and B. It will compute and optimize the full mutual information rather than correlation measures; and also it does not require assumptions on the statistics of an ensemble of spectra but can provide an assessment on individual spectra.

As another related approach, Refs. [14–16] use information theory to estimate various types of information specifically ascribable to colors in images. This approach relies on sampling statistics for the colors, estimated from large amounts of pixels measured in images of scenes under different illumination conditions. As recognized in [16], the amount of information depends on how information is calculated, and the model we develop here relies on quite different statistical assumptions for light spectra. Yet, we will demonstrate that a consistent informational description can also be obtained in this way.

In the present report, we will present the derivation of the original model for trichromacy in Sec. 2. Next, in Sec. 3, the model will be tested for the evaluation of different conceivable trichromatic sensors, and then an application will be described in the context of hyperspectral imaging for plant science.

2. The Informational Model

The light spectrum $S(\lambda)$ as evoked in the introduction commonly measures an energy or power radiated per unit wavelength locally at each wavelength λ. For the present statistical modeling, we choose to count photons, and so by dividing by the energy hc/λ carried by a photon with wavelength λ, we rather define a light spectrum $S(\lambda)$ as a number of photons radiated per unit wavelength locally at each wavelength λ. Moreover, the spectrum $S(\lambda)$ counting the radiated photons is appropriately normalized so that when a photon is emitted by the radiating source, this photon as a probability $S(\lambda)d\lambda$ of being radiated with the wavelength λ, or more precisely in the infinitesimal range $[\lambda, \lambda + d\lambda[$. This assumption for the photon is consistent with the specifications of quantum optics [23]. Also, at a macroscopic level, when a very large number N of photons are radiated by the source, by the law of large numbers, a fraction $NS(\lambda)d\lambda$ is radiated at wavelength λ, which consistently matches our previous interpretation of the spectrum (prior to normalization) as counts of radiated photons per unit wavelength. So the normalized spectrum $S(\lambda)$ is the probability density for a radiated photon to have wavelength λ.

The light is collected by a sensor incorporating a set of photodetectors of M distinct types labeled by index i. We focus here on the important case of trichromacy with $M = 3$, which is specially relevant for the human visual system, yet the model we develop is applicable for arbitrary M [27, 28]. With sensors like RGB

cameras or the human retina, each photodetector i produces an output response usually constructed as a weighted linear integration on the input light. Photodetector i integrates the energy contained in the incident light spectrum weighted by the spectral sensitivity of the photodetector to output a scalar measurement. For our purpose, it is appropriate to also model the response of each photodetector at the level of individual photons and in a probabilistic framework. We consider that each photon with wavelength λ falling on the sensor has a probability $f_i(\lambda)$ of being detected by a photodetector i. The probability $f_i(\lambda)$ is wavelength-dependent to account for a wavelength-dependent spectral sensitivity for each photodetector i. When a very large number N of photons are radiated by the source and fall on the sensor, a fraction $NS(\lambda)d\lambda$ is radiated at wavelength λ, among which a fraction $f_i(\lambda)NS(\lambda)d\lambda$ is detected by a photodetector i. By integration over the whole wavelength range $[\lambda_{\min}, \lambda_{\max}]$ where the input spectrum $S(\lambda)$ contains energy, the total number N_i of photons collected by photodetector i comes out as:

$$N_i = \int_{\lambda_{\min}}^{\lambda_{\max}} f_i(\lambda)NS(\lambda)d\lambda, \quad i = 1, \ldots, M, \tag{1}$$

which matches the macroscopic picture of a weighted integration of the incident light to construct the global response of the photodetector.

A given sensor with spectral resolution capabilities incorporates M distinct photodetector types with M distinct probabilistic spectral sensitivities $f_i(\lambda)$, like the $M = 3$ types of cone photoreceptors in the human retina or the three-CCD of an RGB camera. Consistency of the probabilistic description imposes

$$P_{\text{det}}(\lambda) = \sum_{i=1}^{M} f_i(\lambda) \leq 1, \tag{2}$$

for each λ, where $P_{\text{det}}(\lambda)$ in Eq. (2) is the global probability for an incident photon at λ to be detected by the sensor, altogether by absorption by one of its M internal photodetectors. In addition,

$$P_{\text{lost}}(\lambda) = 1 - P_{\text{det}}(\lambda) = 1 - \sum_{i=1}^{M} f_i(\lambda), \tag{3}$$

is the probability that an incident photon at λ is missed by the sensor.

For instance, a useful model of spectral sensitivity [29–31] is according to the Gaussian

$$f_i(\lambda) = A_i \exp\left[-\left(\frac{\lambda - \lambda_i}{w_i}\right)^2\right]. \tag{4}$$

For each photon we denote by Y the random variable describing the photodetection event occurring in the sensor. A photon emitted by the source is emitted at wavelength λ with the probability $S(\lambda)d\lambda$; and a photon at λ is absorbed by photodetector i with the (conditional) probability $P(Y = i \,|\, \lambda) = f_i(\lambda)$. By integration

over the whole wavelength range, we obtain the overall probability that a photon emitted by the source is detected by photodetector i as:

$$P(Y=i)=\int_{\lambda_{\min}}^{\lambda_{\max}} f_i(\lambda)S(\lambda)d\lambda, \quad i=1,\ldots,M, \tag{5}$$

consistent with the global count N_i of Eq. (1). There is also a possibility that the photon at λ is missed that we denote $Y=0$, occurring according to Eq. (3) with (conditional) probability $P(Y=0\,|\,\lambda)=P_{\text{lost}}(\lambda)$, leading to the overall probability of a lost photon as

$$P(Y=0)=\int_{\lambda_{\min}}^{\lambda_{\max}} P_{\text{lost}}(\lambda)S(\lambda)d\lambda. \tag{6}$$

In this way, the detection of a photon falling on the sensor is modeled as a random event Y, with $M+1$ possible outcomes, consisting in a detection by photodetector i with the probability $P(Y=i)$ of Eq. (5) for $i=1$ to M, or in a lost photon with the probability $P(Y=0)$ of Eq. (6).

We can now define the entropy $H(Y)$ of the detection process as [13]

$$H(Y)=-\sum_{i=0}^{M} P(Y=i)\log[P(Y=i)]. \tag{7}$$

In a similar way, the emission of a photon by the light source can be modeled as a random event X which describes the wavelength λ at which this photon is emitted, with the outcome $X\in[\lambda,\lambda+d\lambda[$, or more concisely $X=\lambda$, occurring with probability

$$\Pr\{X\in[\lambda,\lambda+d\lambda[\,\}=S(\lambda)d\lambda. \tag{8}$$

The process of representing a continuous spectrum $S(\lambda)$ by the scalar measurements delivered by the M photodetectors, can thus be described as an information channel, with input X and output Y. An input–output mutual information $I(X;Y)$ can be defined for such a channel, as [13]

$$I(X;Y)=H(Y)-H(Y\,|\,X), \tag{9}$$

with $H(Y)$ the output entropy of Eq. (7), and the input–output conditional entropy

$$H(Y\,|\,X)=\int_{\lambda_{\min}}^{\lambda_{\max}} H(Y\,|\,X=\lambda)S(\lambda)d\lambda. \tag{10}$$

From the above description of operation of the photodetectors, we have

$$H(Y\,|\,X=\lambda)=-\sum_{i=0}^{M} P(Y=i\,|\,X=\lambda)\log[P(Y=i\,|\,X=\lambda)], \tag{11}$$

which is

$$H(Y\,|\,X=\lambda)=-\sum_{i=1}^{M} f_i(\lambda)\log[f_i(\lambda)]-P_{\text{lost}}(\lambda)\log[P_{\text{lost}}(\lambda)]. \tag{12}$$

Then, gathering Eqs. (12), (10) and (7) gives access to the mutual information $I(X;Y)$ in Eq. (9). As visible, the resulting mutual information $I(X;Y)$ critically depends on the spectral sensitivities $f_i(\lambda)$ of the photodetectors. In this way, $I(X;Y)$ offers a quantitative assessment, in informational terms, of the process of representing the continuous input spectrum $S(\lambda)$ by the discrete scalar measurements from M photodetectors.

The present model is based on assigning a probabilistic interpretation to the spectral quantities that control the photon statistics determining the informational measures. As already mentioned, this is an approach bearing similarity with that of [19, 20, 22], and interpreting light intensity as a probabilistic measure. This similarity provides *a priori* motivation to our approach, which transposes to the spectral domain the probabilistic approach fruitfully developed in [19, 20, 22] for light distribution in the spatial domain. An important step now, for the model we have derived, is to test its properties, capabilities and informational significance. We now address and illustrate these aspects, especially to provide additional, *a posteriori*, motivation to our informational analysis.

3. Application of the Model

3.1. *An idealized trichromatic sensor*

An idealized trichromatic sensor specially efficient for spectral discrimination according to the present informational approach, would use three rectangular sensitivities $f_i(\lambda) = 1$ over nonoverlapping wavelength supports and $f_i(\lambda) = 0$ outside. Such rectangular $f_i(\lambda)$ at 0 or 1 cancel the conditional entropy $H(Y \mid X = \lambda)$ of Eq. (12) for any λ, and thus yield $H(Y \mid X) = 0$ in Eq. (10) which is the overall minimum of the nonnegative conditional entropy $H(Y \mid X)$. At the same time, these rectangular $f_i(\lambda)$ are able to achieve the overall maximum $\log(M + 1)$ for the output entropy $H(Y)$ in Eq. (7). This is realized, for a given input spectrum $S(\lambda)$, by placing the spectral supports of the rectangular sensitivities $f_i(\lambda)$ so as to obtain equiprobable $P(Y = i) = 1/(M + 1)$ for $i = 0$ to M in Eq. (7). This guarantees the overall maximum of the mutual information $I(X;Y)$ in Eq. (9). These rectangular sensitivities *a priori* stand as a reasonable intuitive expectation for what can represent a form of efficient trichromatic sensor; and *a posteriori* they also stand as the optimum predicted by the informational approach. This provides ground to the informational approach, which matches reasonable intuitive solutions whenever they are accessible.

However the rectangular sensitivities, with perfectly flat response at the maximum sensitivity $f_i(\lambda) = 1$ and infinitely sharp selectivity at the support boundaries, display an idealized character. They may not correspond to physically realizable solutions, as for instance the sensitivities $f_i(\lambda)$ accessible with current technologies of photodetectors or with biophysical devices such as the cone photoreceptors in the retina. We therefore extend the exploration of the capabilities of the informational

model in this direction of sensors constrained so as to come closer to more realistic physical conditions.

3.2. *A simple trichromatic sensor*

We turn to a smoother model of spectral sensitivities $f_i(\lambda)$, with no discontinuities, yet simple enough to be amenable to quantitative analysis and qualitative understanding. We introduce the function $\mathrm{tri}(x)$ as a symmetric (even) triangular waveform of magnitude unity and support $x \in [-1, 1]$, and zero elsewhere, according to

$$\mathrm{tri}(x) = \begin{cases} 1 - |x| & \text{for } x \in [-1, 1], \\ 0 & \text{otherwise.} \end{cases} \tag{13}$$

We take

$$f_i(\lambda) = \mathrm{tri}\left(\frac{\lambda - \lambda_i}{w_i}\right) \tag{14}$$

as the triangular waveform centered at λ_i with support in $[\lambda_i - w_i, \lambda_i + w_i]$. Figure 1 depicts three spectral sensitivities $f_i(\lambda)$ according to the triangular model of Eq. (14), with different parameter settings (λ_i, w_i), in a way which could crudely mimic the situation of a trichromatic sensor like the retina or an RGB camera.

As a common model for a light spectrum, we consider a black body spectrum according to the Planck law as [23]

$$B(\lambda) = \frac{2hc^2}{\lambda^5} \frac{1}{\exp\left(\frac{hc}{kT\lambda}\right) - 1}. \tag{15}$$

At a temperature $T = 6000\,\mathrm{K}$, the black body spectrum $B(\lambda)$ of Eq. (15) is a good model for the solar illumination on earth. The energetic spectrum $B(\lambda)$ of

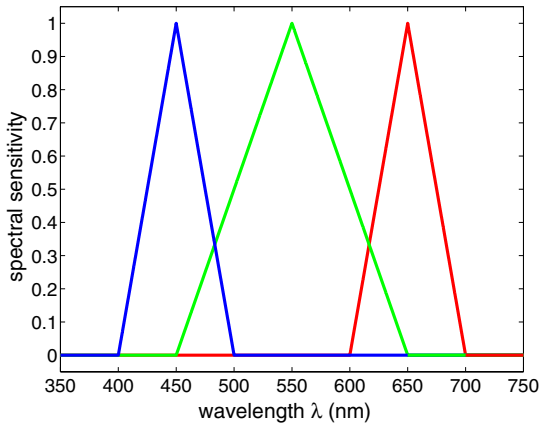

Fig. 1. For a trichromatic sensor, the three spectral sensitivities $f_i(\lambda)$ according to the triangular model of Eq. (14) with, from left to right, in nanometers $(\lambda_1 = 450, w_1 = 50)$, $(\lambda_2 = 550, w_2 = 100)$ and $(\lambda_3 = 650, w_3 = 50)$.

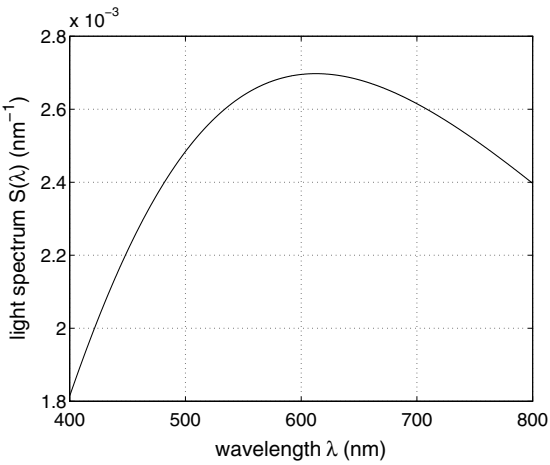

Fig. 2. Input spectrum $S(\lambda)$ resulting from the black body spectrum $B(\lambda)$ of Eq. (15) at temperature $T = 6000\,\mathrm{K}$ normalized over the visible range $\lambda \in [\lambda_{\min} = 400\,\mathrm{nm}, \lambda_{\max} = 800\,\mathrm{nm}]$.

Eq. (15), after division by hc/λ to obtain a number of photons, and after proper normalization as explained in Sec. 2, leads to the spectrum $S(\lambda)$ depicted in Fig. 2. The black body spectrum will serve here as an interesting model of broadband light spectrum useful to test the present informational modeling of trichromacy.

We now want to analyze the coding of the black body spectrum of Fig. 2 by the trichromatic sensor of Fig. 1. Especially, the input–output mutual information $I(X;Y)$ from Eq. (9) offers a measure of efficacy of this coding, enabling for instance to appreciate the impact on the coding of the parameterization (λ_i, w_i) of the photodetectors. For illustration, we consider that the parameters (λ_i, w_i) are fixed as in Fig. 1 except for the spectral width w_2 of the green photodetector which is assumed adjustable. Then, Fig. 3 shows the input–output mutual information $I(X;Y)$ resulting from Eq. (9), as a function of the adjustable width w_2 of the spectral sensitivity $f_2(\lambda)$ of the green photodetector.

The evolution in Fig. 3 reveals that there exists a maximum of the mutual information $I(X;Y)$, which is achieved by an optimal width $w_2 = 100\,\mathrm{nm}$ for the spectral sensitivity of the green photodetector of the trichromatic sensor in Fig. 1. The spectral sensitivity of the green photodetector is depicted in Fig. 1 at this optimal width $w_2 = 100\,\mathrm{nm}$ achieving the maximum $I(X,Y) = 1.0790\,\mathrm{Sh}$. Figure 1 represents the optimal sensor in the constrained family of sensors with spectral sensitivities according to Eq. (14) and one adjustable parameter w_2. The optimum of Fig. 1 predicts that the trichromatic sensor of Fig. 1 is maximally efficient when there is some overlap, in the wavelength domain, of the spectral sensitivities $f_i(\lambda)$ of its three types of photodetectors. Especially, the configuration with $w_2 = 50\,\mathrm{nm}$ that would correspond to three sensitivities $f_i(\lambda)$ of equal width and no overlap in Fig. 1, is not optimal, according to the mutual information measure. This is in

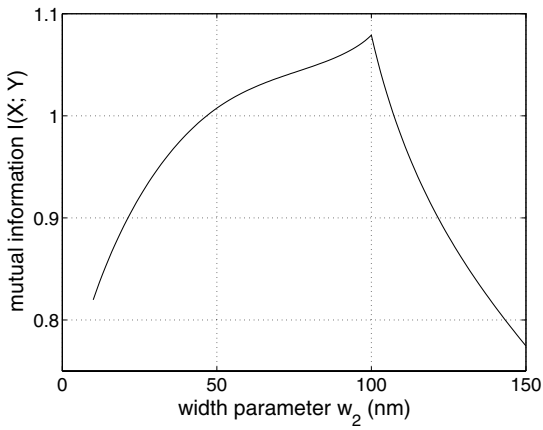

Fig. 3. For the coding of the black body spectrum of Fig. 2 by the trichromatic sensor of Fig. 1, input–output mutual information $I(X;Y)$ from Eq. (9), as a function of the adjustable width w_2 of the spectral sensitivity $f_2(\lambda)$ of the green photodetector.

contrast with the flat sensitivities of Sec. 3.1 which are optimal with no overlap. The graded sensitivities of Eq. (14) draw benefit from some overlap for better spectral representation.

The special case of a monochromatic light can illustrate that some benefit can be drawn from the overlap of graded sensitivities as in Fig. 1. A monochromatic light, from which a large number of photons is collected, when there is no overlap of the three sensitivities $f_i(\lambda)$ will be represented by an $(\mathrm{R},\mathrm{G},\mathrm{B})$ triplet with only one nonzero component among three. Such configurations realize a limited exploitation of the representation capabilities of a triplet (R, G, B), associated with an output variable Y with a low entropy $H(Y)$ in Eq. (7) and a low input–output mutual information $I(X;Y)$ in Eq. (9). Some overlap in the sensitivities $f_i(\lambda)$ will produce triplets $(\mathrm{R},\mathrm{G},\mathrm{B})$ with more than one nonzero components, exploiting a larger part of the representation capabilities of a triplet $(\mathrm{R},\mathrm{G},\mathrm{B})$, associated with higher output entropy $H(Y)$ in Eq. (7) and higher input–output mutual information $I(X;Y)$ in Eq. (9). The overlap coupled to graded sensitivities preserve the localization capabilities of the sensor (which is not true with the flat sensitivities of Sec. 3.1). For instance, a monochromatic light at $\lambda_0 \approx 480\,\mathrm{nm}$ activates the blue and green photodetectors in the same way, since $f_1(\lambda_0) \approx f_2(\lambda_0) \approx 0.3$ in Fig. 1, and is thus represented by a triplet $(\mathrm{R},\mathrm{G},\mathrm{B})$ with $\mathrm{B} = \mathrm{G}$ and $\mathrm{R} = 0$. This same proportion of B and G precisely locates the monochromatic light at $\lambda_0 \approx 480\,\mathrm{nm}$ in Fig. 1. Other proportions of R, G and B would usually allow similar capability of precisely locating another λ_0 from the overlapping graded sensitivities of Fig. 1. This special case of a monochromatic light offers a concrete illustration of the possibility of some benefit from overlap in graded spectral sensitivities, as pointed out by maximization of the input–output mutual information $I(X;Y)$. The case of a broadband spectrum

$S(\lambda)$ is more complex than that of the monochromatic light. However, one can expect that the measure $I(X;Y)$ with its general informational significance, keeps some relevance to assess spectral representation in wide conditions. On a general basis, for overlapping sensitivities $f_i(\lambda)$, maximization of the input–output mutual information $I(X;Y)$ in Eq. (9), realizes an optimal trade-off between output richness of representation measured by $H(Y)$ and input–output equivocation measured by $H(Y\,|\,X)$. The whole shapes of the sensitivities $f_i(\lambda)$, and not only the overlap of their supports, is taken into account in the maximization of $I(X;Y)$, so as to provide an information-based optimum for the setting of adjustable parameters in the spectral sensitivities $f_i(\lambda)$.

3.3. *Gaussian trichromatic sensor*

As another example of the optimization capabilities of the informational model, we address the situation of a Gaussian trichromatic sensor with three types of photodetectors with Gaussian spectral sensitivities $f_i(\lambda)$ as in Eq. (4). We consider the case where the spectral widths w_i in Eq. (4) are fixed to the common value $w_i = 50\,\text{nm}$, for $i = 1, 2, 3$, which is typical to commercial trichromatic cameras [31]. It is then feasible to use the informational approach to optimize the locations λ_i and relative magnitudes A_i in Eq. (4), by seeking those values that maximize the input–output mutual information $I(X, Y)$. This is done again with the black body spectrum of Fig. 2 as input, and the resulting optimal sensitivities are presented in Fig. 4 that achieves the maximum $I(X, Y) = 1.2495\,\text{Sh}$.

The optimal configuration of the trichromatic sensor in Fig. 4 shows that there is significant overlap of the spectral sensitivities $f_i(\lambda)$ at the optimum. The central

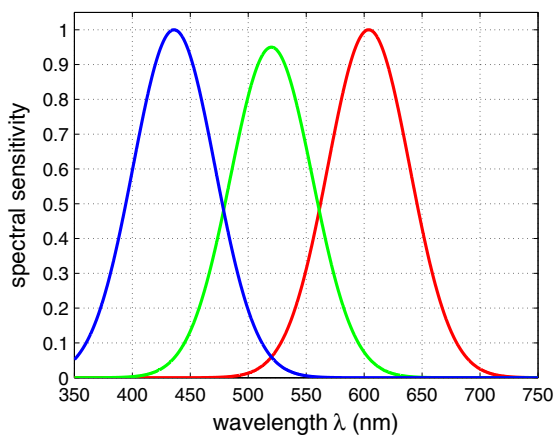

Fig. 4. For the coding of the black body spectrum of Fig. 2 by a trichromatic sensor with Gaussian spectral sensitivities $f_i(\lambda)$ as in Eq. (4) and $w_i = 50\,\text{nm}$, for $i = 1, 2, 3$, the optimal configuration $(A_1 = 1, \lambda_1 = 436\,\text{nm})$, $(A_2 = 0.95, \lambda_2 = 520\,\text{nm})$ and $(A_3 = 1.00, \lambda_3 = 604\,\text{nm})$, maximizing the input–output mutual information $I(X;Y)$ from Eq. (9).

(green) spectral sensitivity $f_2(\lambda)$ has a slightly lower relative magnitude $A_2 = 0.95$ at the optimum in Fig. 4, which is consistent to cover the middle-wavelength range where the three sensitivities $f_i(\lambda)$ overlap most. For the coding of the black body spectrum of Fig. 2, the optimized sensor with Gaussian sensitivities of Fig. 4 achieving $I(X,Y) = 1.2495\,\text{Sh}$, is a little more efficient than the optimized sensor with triangular sensitivities of Fig. 1 which achieves $I(X,Y) = 1.0790\,\text{Sh}$, according to the present informational criterion.

3.4. *Photopic vision in the retina*

We now study with the informational model, the trichromatic sensor formed by the human retina for photopic vision. For the characterization of the three types of cone photoreceptors of the retina, numerical values estimated for the effective sensitivities were taken from [32, p. 8]. Then for our purpose here, we have fit the numerical values from [32] with the three theoretical models, given for the S, M and L cones respectively by Eqs. (16)–(18), where the wavelength λ is in nanometers:

$$f_1(\lambda) = \left(\frac{\lambda - 381}{26.8}\right)^{7.2} \exp\left[-\left(\frac{\lambda - 381}{15}\right)^{1.2}\right], \quad \lambda \geq 381\,\text{nm}; \tag{16}$$

$$f_2(\lambda) = 1.1 \exp\left[-\left(\frac{\lambda - \lambda_2}{w_2}\right)^2\right], \quad (\lambda_2, w_2) = (549, 54)\,\text{nm}; \tag{17}$$

$$f_3(\lambda) = 0.97 \exp\left[-\left(\frac{\lambda - 573}{61}\right)^2\right]. \tag{18}$$

The three spectral sensitivities $f_i(\lambda)$ of Eqs. (16)–(18) are then plotted in Fig. 5.

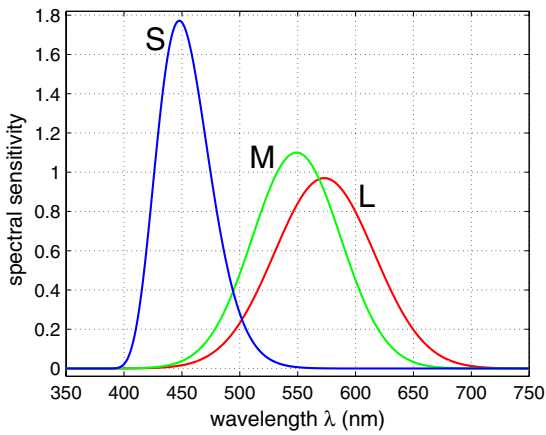

Fig. 5. For the S, M and L cone photoreceptors of the human retina, the three theoretical models of spectral sensitivities, respectively $f_1(\lambda)$, $f_2(\lambda)$ and $f_3(\lambda)$ according to Eqs. (16)–(18), and matching the estimated numerical values from [32].

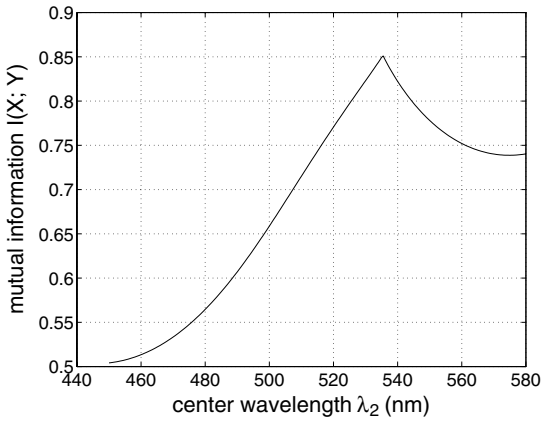

Fig. 6. For the coding of the black body spectrum of Fig. 2 by the trichromatic sensor (retina) of Fig. 5, input–output mutual information $I(X;Y)$ from Eq. (9), as a function of the adjustable center wavelength λ_2 of the spectral sensitivity $f_2(\lambda)$ from Eq. (17).

We can now apply the mutual information measure of Sec. 2, for an assessment of the retina operating with the photoreceptors of Fig. 5. It is possible for instance to evaluate the impact of the center wavelength λ_2 of the spectral sensitivity $f_2(\lambda)$ from Eq. (17). In Fig. 6, the center wavelength λ_2 of the type M cone is varied between 450 and 580 nm, and the resulting mutual information $I(X;Y)$ is presented.

The mutual information $I(X;Y)$ in Fig. 6 displays a maximum for the center wavelength $\lambda_2 = 535\,\text{nm}$. This indicates that, according to the mutual information measure in Fig. 6, the nominal position $\lambda_2 = 549\,\text{nm}$ as in Eq. (17), is not optimal for the center wavelength. Instead, $\lambda_2 = 535\,\text{nm}$ is the one-parameter optimized configuration maximizing the input–output mutual information in the trichromatic representation.

Figure 7 shows the assessment of the spectral width parameter w_2 of the sensitivity $f_2(\lambda)$ of the type M cone from Eq. (17).

The mutual information measure in Fig. 7, shows that the nominal configuration $w_2 = 54\,\text{nm}$ as in Eq. (17), is not optimal for the spectral width. Instead, $w_2 = 79\,\text{nm}$ is the one-parameter optimized configuration in Fig. 7 for maximizing the input–output mutual information in the trichromatic representation.

For the spectral sensitivity $f_2(\lambda)$ of Eq. (17), when both parameters λ_2 and w_2 are assumed adjustable. Figure 8 presents the input–output mutual information $I(X;Y)$ in the plane (λ_2, w_2).

The joint optimization in (λ_2, w_2) maximizing the mutual information $I(X,Y)$ in Fig. 8, leads to the optimal configuration $(\lambda_2 = 533, w_2 = 48)\,\text{nm}$ associated with the maximum $I(X,Y) = 0.86\,\text{Sh}$. The resulting optimal sensitivity $f_2(\lambda)$ is depicted in Fig. 9.

Only the low-level operation of forming the trichromatic representation is assessed in Fig. 9, and specifically by means of the proposed informational criterion,

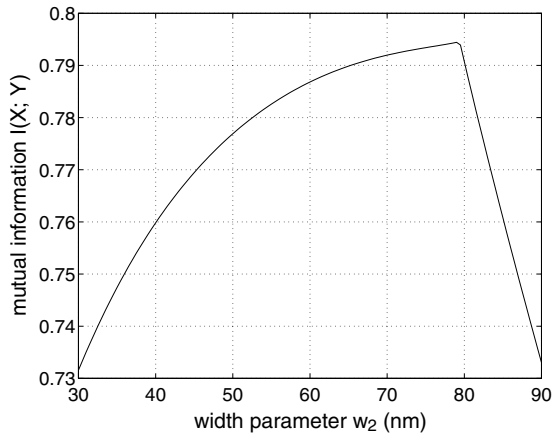

Fig. 7. For the coding of the black body spectrum of Fig. 2 by the trichromatic sensor (retina) of Fig. 5, input–output mutual information $I(X;Y)$ from Eq. (9), as a function of the adjustable width parameter w_2 of the spectral sensitivity $f_2(\lambda)$ from Eq. (17).

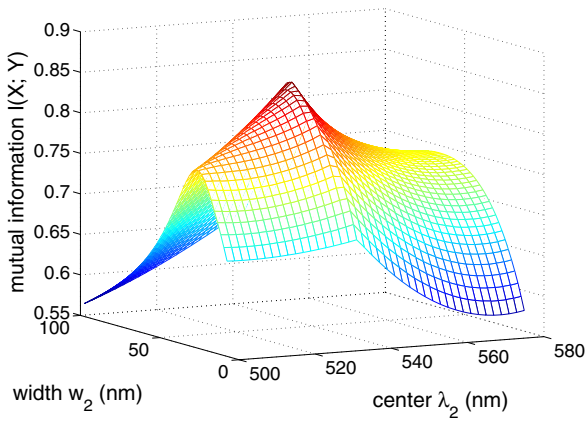

Fig. 8. For the coding of the black body spectrum of Fig. 2 by the trichromatic sensor (retina) of Fig. 5, input–output mutual information $I(X;Y)$ from Eq. (9), as a function of the center wavelength λ_2 and width w_2 of the spectral sensitivity $f_2(\lambda)$ from Eq. (17).

and optimization is performed over a small set of adjustable parameters to illustrate the approach. The results of Fig. 9 do not imply a deficiency in the human visual system, because as a whole, the human visual system integrates more complex and higher levels of information processing of the color information which are not addressed by the present informational model of trichromacy. The operation of the retina itself may be optimized based on different aspects, and related to the visual system as a whole. Our goal here is not the modeling of color processing by the visual system. It is rather an informational modeling of the process of representing

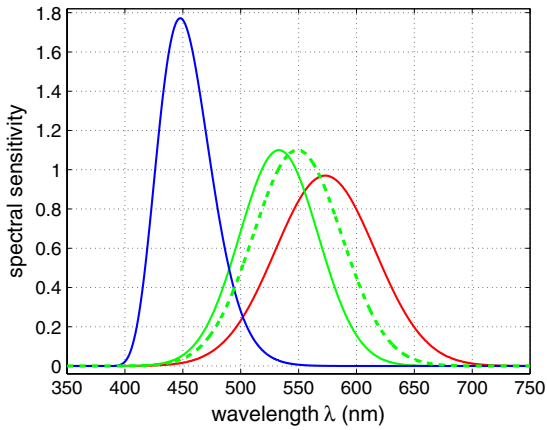

Fig. 9. For the S, M and L cones of the retina, the models of spectral sensitivities from Fig. 5 and after optimization at $(\lambda_2 = 533, w_2 = 48)$ nm of the M cone sensitivity $f_2(\lambda)$ in Eq. (17) maximizing in Fig. 8 the input–output mutual information $I(X, Y)$ (solid lines). The dashed line is the non-optimal nominal configuration $(\lambda_2 = 549, w_2 = 54)$ nm for $f_2(\lambda)$ as in Fig. 5.

a continuous light spectrum by three scalar (trichromatic) components, with an assessment of the efficiency of the process in informational terms.

Nevertheless, the optimal configuration $(\lambda_2 = 533, w_2 = 48)$ nm according to the information-theoretic model, and the nominal configuration $(\lambda_2 = 549, w_2 = 54)$ nm of the retina, as compared in Fig. 9, can be interpreted as close to one another, with respect to the ranges where the parameters (λ_2, w_2) can have meaningful variations. It can then be concluded that, for the coding of a black body spectrum representing the average solar illumination on earth, the tuning of the retina is close to an optimum according to the present information-theoretic model. This somehow confirms that biological sensory organs are adapted in their environment for efficient information processing. In the reverse direction, one can *a priori* grant some form of optimality for information processing to the retina, due to its being the result of a selection process refined over biological evolution [10, 11]. Then the information-theoretic model which arrives at an optimum close to the biological solution, receives in this way some legitimation for its ability to convey a meaningful notion of informational optimality. Altogether, one can retain here some form of consistency uniting sensory processing and informational modeling.

3.5. *An application to hyperspectral images*

We now propose an illustration of the informational model on experimentally measured light spectra from hyperspectral imaging. We consider an application from plant science for the detection of apple scab [33, 34]. Apple scab is a major infectious agent damaging the production of apples. Early detection of apple scab on the tree leaves prior to propagation to the fruits is an important challenge for yield

improvement. The proposal here is to apply our informational model of trichromacy in order to produce an optimized representation of light spectra measured from apple tree leaves, and test the potential of this optimal trichromatic representation for early detection of apple scab.

In order to assess various possible trichromatic representations, we start in the laboratory with the measurement of high-resolution spectra. We used a NEO HySpex hyperspectral camera capable of measuring spectra with 160 equal-width bands over the wavelength range $\lambda \in [\lambda_{\min} = 400\,\text{nm}, \lambda_{\max} = 1000\,\text{nm}]$ corresponding to a spectral resolution $\Delta\lambda = 3.75\,\text{nm}$, with a 12-bit quantization. Such high-resolution spectra are then used to compute a trichromatic representation through linear integration weighted by a set of three spectral sensitivity functions $f_i(\lambda)$ chosen for the three types of photodetectors. In this way, from a measured hyperspectral image in which each pixel is a 160-component high-resolution spectrum, we construct a pseudo RGB image in which each pixel is a 3-component vector representation which can be handled and displayed as a standard RGB image. Figure 10 displays three such trichromatic images constructed from a high-resolution hyperspectral image of an apple tree leaf infected by scab. The three trichromatic images of Fig. 10 are constructed through weighted integration by three different sets of spectral sensitivities $\{f_i(\lambda), i = 1, 2, 3\}$.

The trichromatic image of Fig. 10(a) is computed with the set of spectral sensitivities $\{f_i(\lambda), i = 1, 2, 3\}$ from Eqs. (16)–(18) modeling the photodetectors of the retina. The trichromatic image of Fig. 10(a) is very close in appearance to the leaf

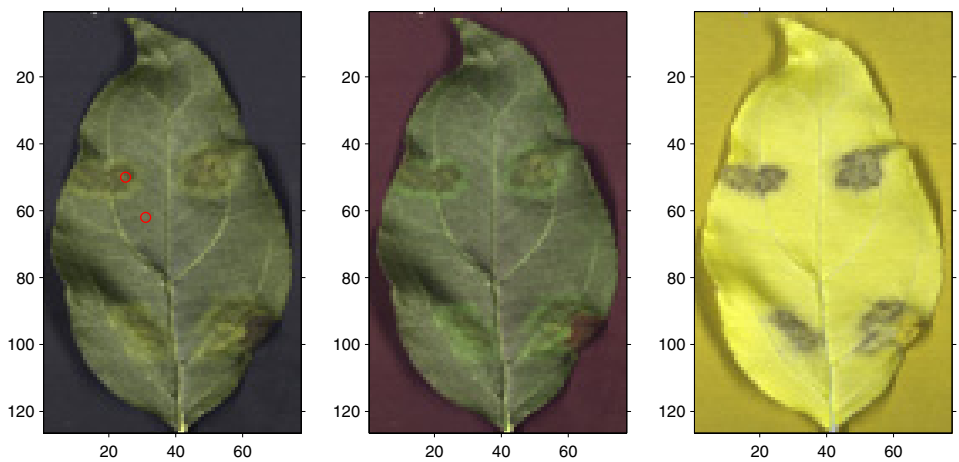

Fig. 10. Three trichromatic images with size 77×126 pixels, from a high-resolution hyperspectral image of an apple tree leaf infected by scab, constructed through weighted integration by three different sets in (a), (b) and (c), of spectral sensitivities $\{f_i(\lambda), i = 1, 2, 3\}$. In (a) the two red circles at pixels $(25, 50)$ and $(31, 62)$ indicate the spots of the two spectra displayed in Fig. 11.

as it appears to the naked eye. The trichromatic image of Fig. 10(b) is computed with three Gaussian spectral sensitivities $f_i(\lambda)$ according to Eq. (4), with equal width $w_i = 50\,\text{nm}$, equal magnitude $A_i = 1$, and evenly covering the visible spectrum with center wavelengths at $\lambda_1 = 450\,\text{nm}$, $\lambda_2 = 550\,\text{nm}$ and $\lambda_3 = 650\,\text{nm}$. The trichromatic image of Fig. 10(b) realizes an RGB image as it could be produced by a standard RGB camera operating over the visible wavelength range.

For the purpose of the experiment, scab has been deliberately inoculated onto the leaf of Fig. 10 in four known areas. The two images of Figs. 10(a) and 10(b) illustrate that the infection by scab is barely visible, by the naked eye of by a standard RGB camera, as also known from previous studies [33, 34]. In order to improve the detection of apple scab, we now devise a third trichromatic representation, as shown in Fig. 10(c), optimized according to our informational model of trichromacy.

A high-resolution spectrum representative of an infected region on the leaf is extracted from the hyperspectral image. Such a spectrum representative of an infected region is plotted in Fig. 11, together with another spectrum representative of a sane region of the leaf. The two spots of measurement, at pixels $(25, 50)$ and $(31, 62)$ in the hyperspectral image, are indicated by two red circles in Fig. 10(a).

The experimental spectra are used in the computation with their native resolution $\Delta\lambda$ corresponding to 160 regular spectral bands over the integration domain $\lambda \in [\lambda_{\min} = 400\,\text{nm}, \lambda_{\max} = 1000\,\text{nm}]$ and a 12-bit quantization, this providing an adequate representation of the smoothly varying measured spectra, as observed in Fig. 11. By comparison, the black body spectrum used in Secs. 3.2–3.4 from the model of Eq. (15) was sampled, for numerical evaluation of the integrals as Eqs. (5)–(6), with a very narrow step typically to accommodate 10^4 regular samples over the integration domain $[\lambda_{\min}, \lambda_{\max}]$. The quantization is at the resolution

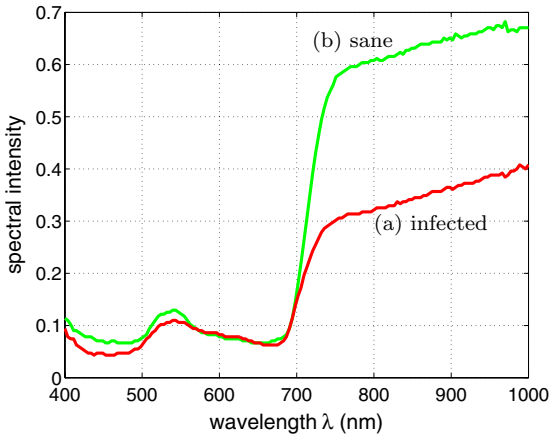

Fig. 11. Two representative spectra from the hyperspectral image of Fig. 10: (a) (in red) at pixel $(25, 50)$ in the infected region; (b) (in green) at pixel $(31, 62)$ in the sane region.

of modern computers for number representation, just as for the discrete probabilities $P(Y = i)$ resulting from the input spectra. Such conditions in themselves are generally not critical for the study.

It can be observed in Fig. 11 that the two measured spectra representative of a sane or an infected regions are relatively poorly contrasted over the visible range up to $\lambda \approx 700\,\text{nm}$. This explains the relatively low efficiency of the two images of Figs. 10(a) and 10(b) for distinguishing the infection by scab on the leaf. Meanwhile, in the near infrared range above 700 nm in Fig. 11, the contrast of the sane and infected spectra is much more pronounced. Also, we have verified that the infected spectrum shown in Fig. 11(a) is well representative of the spectra at pixels known to be infected in the hyperspectral image, with relatively low dispersion among them compared to the variability of the spectra over the whole leaf. For the task of constructing a trichromatic image offering a good display of the infected regions of the leaf, we choose to optimize the trichromatic representation according to the informational approach of Sec. 2 with the infected spectrum of Fig. 11(a) as input. Three Gaussian spectral sensitivities $f_i(\lambda)$ according to Eq. (4), with adjustable parameters (λ_i, w_i, A_i) for $i = 1$ to 3, are chosen for the trichromatic sensor. The input–output mutual information $I(X;Y)$ is then maximized according to the nine parameters (λ_i, w_i, A_i) for $i = 1$ to 3. The optimal configuration maximizing $I(X;Y)$ is depicted in Fig. 12.

For maximization of $I(X;Y)$ over a small number of parameters, direct computation of $I(X;Y)$ over a fine grid of points in the parameter space is usually feasible. This provides an evaluation of the criterion $I(X;Y)$ as shown in Figs. 3, 6, 7 for a

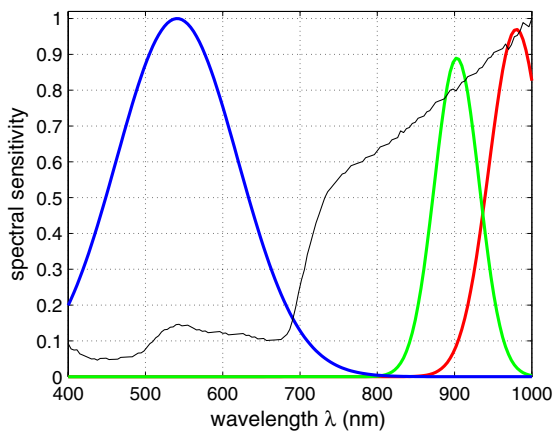

Fig. 12. Three optimal Gaussian spectral sensitivities according to Eq. (4) and jointly maximizing the input–output mutual information $I(X,Y)$ for the infected spectrum represented by the black thin line (the spectrum of Fig. 11(a) converted to a number of photons by division by hc/λ and normalized to unit magnitude to fit into the figure): $(\lambda_1 = 541, w_1 = 111, A_1 = 1)$, $(\lambda_2 = 903, w_2 = 41, A_2 = 0.89)$, $(\lambda_3 = 980, w_3 = 50, A_3 = 0.97)$ achieving $I(X,Y) = 1.2109\,\text{Sh}$.

one-parameter space, and in Fig. 8 for a two-parameter space, from which a location for the maximum is easily deduced. For maximization of $I(X;Y)$ over a larger number of parameters as in Fig. 12, direct computation of $I(X;Y)$ is feasible only over loose or reduced grids in the parameter space. For maximization of $I(X;Y)$ in Fig. 12, we fixed $A_1 = 1$ with no loss of generality since the informational criterion is insensitive to a common magnitude of reference for the three spectral sensitivities $f_i(\lambda)$. Also the variation of the center wavelengths is limited by the condition $\lambda_1 \leq \lambda_2 \leq \lambda_3$ with no loss of generality. For maximization of $I(X;Y)$ over the remaining parameters (λ_i, w_i, A_i) we combined several techniques having simple implementations. We used multidimensional line search methods [35, 36] combined with direct computation of the criterion over successively reduced domains; and these approaches were repeated with several initializations and parameterizations, and various perturbations of the solution to test its robustness [35]. The resulting maximum associated with Fig. 12 is obtained with a spectral precision consistent with the spectral resolution $\Delta\lambda$ of the measured spectra in Fig. 11. Alternative techniques can be used for maximizing the informational criterion $I(X;Y)$. For our main purpose here of presenting the informational model of trichromacy, a validation of the interest of the solution obtained in Fig. 12 rests also in the enhanced representation afforded by the resulting optimized trichromatic image of Fig. 10(c).

The optimal spectral sensitivities in Fig. 12 tend to concentrate in the range of high wavelengths where the input spectrum has larger magnitude and larger number of photons. At the same time, some uniform representation of the whole input spectrum over its whole support between 400 nm and 1000 is preserved, with the blue sensor $f_1(\lambda)$ insuring a broadband integration to convey the low-magnitude spectral features present in the lower range of the support. A significant outcome of the informational optimization realized in Fig. 12, is the resulting trichromatic image of the leaf which is represented in Fig. 10(c). It can be realized in Fig. 10 that the visibility of the four infected regions (appearing darker in Fig. 10(c)) has been significantly enhanced. This is automatically achieved by the numerical criterion of the maximization of the input–output mutual information $I(X;Y)$. Yet, as visible from Fig. 10, the numerical criterion expressed with informational quantities also matches a notion of perceived efficiency in the visual inspection for scab detection from a trichromatic image. This provides further motivation and significance to the present informational model of trichromacy.

4. Discussion

We have proposed here an original informational model for trichromacy. The model is based on a statistical analysis of the dynamics of individual photons, and it relies on a probabilistic interpretation of the spectral quantities that control the photon statistics taking place in the operation of a trichromatic sensor. Trichromacy in this way can be described as an information channel for which an input–output mutual information can be computed to serve as a measure of performance. After

the construction of the model here, several applications have been performed which illustrate some of its informational capabilities. The model especially exhibits the influence of the spectral sensitivities of the photodetectors realizing the trichromatic representation, and provides a means to optimize their adjustable parameters with an informational criterion. Other informational models of trichromacy can of course be envisaged, based on other assumptions and a different procedure; yet our approach forms a consistent proposal for an informational model. It is especially not limited by the requirement of large numbers of realizations to be observed from a statistical ensemble which often sets a limit in probabilistic modeling. The results here stand as first exposition and test of the model, and more explorations are under way to further study the informational capabilities of the model in broader conditions.

A specific area of application of the present informational model is the design of low-cost optimized imaging systems. Starting with a hyperspectral camera accessible in the laboratory as in the scenario of Sec. 3.5, one can use the informational model to design a set of optimal photodetector spectral sensitivities selected to maximize the visibility in a scene of objects or regions characterized by a given representative spectrum. The optimization can take into account technological constraints imposed by the available optical components, like photodetectors and their spectral responses, or optical filters, or light sources with their spectral profiles [37, 38]. The result would be a low-cost imaging system, resembling standard RGB imaging systems, yet producing trichromatic images optimized for the efficient observation of objects of interest specified by their broadband reflectance spectrum. Live sciences especially could benefit from such low-cost imaging systems spectrally optimized. Biological structures and tissues from animals or plants can be characterized by specific reflectance spectra. Multispectral and hyperspectral imagings, which were initially focused to remote sensing, are more and more often applied in the laboratory to near-field imaging, especially for characterization in life sciences. These broadband imaging systems remain relatively costly, and could, for some applications, be replaced by low-cost RGB-like trichromatic systems spectrally optimized as described here. This could for instance contribute in the exploitation of the high potential of hyperspectral imaging for plant phenotyping, quality assessment, and early detection of plant pathogens [33, 39–42].

Various extensions of the present informational model of trichromacy can be envisaged. For instance, for further application to imaging, spatial information could also be taken into account to complement the spectral information attached to the light spectra. In the situation of Sec. 3.5 with hyperspectral images, a single spectrum representative of a class of interest for the pixels, is taken into account as input to the model, so as to optimize the trichromatic representation for maximum information transmission regarding this representative spectrum. As an extension, spatial dependence of spectra of interest from a scene could be taken into account. This requires to refine the statistical object (the spectrum) forming the input to the information channel, by including an account of a spatial dimension. This could

be done for instance based on the statistical interpretation of the spatial distribution of light intensities over an image as in the informational approach to imaging of [19, 20, 22, 43]; or also based on histograms as probability distributions constructed from an ensemble of pixels. Also, depending on the task envisaged, informational measures other than the input–output mutual information $I(X;Y)$, could be chosen to assess the performance of the trichromatic representation. For instance in imaging, for a task of classification between two classes of pixels, each class being well characterized by a representative spectrum, an informational measure of class contrast or separation, like the relative entropy or Kullback–Leibler divergence [13], or even richer informational measures applicable in imaging [44, 45], could be considered. An explicit expression for such an informational contrast can be derived in the framework of the model of Sec. 2. The trichromatic representation could then be optimized so as to maximize this informational contrast for a trichromatic image displaying the two classes of interest. Rich potentialities therefore exist to pursue informational approaches in imaging, and to connect physics, biophysics and information theory.

Acknowledgments

We are grateful to Valérie Caffier and Pascale Expert for providing the apple tree leaves with scab. Landry Benoit gratefully acknowledges financial support from Angers Loire Métropole and from GEVES-SNES for the preparation of his PhD.

References

[1] F. A. Bais and J. D. Farmer, The physics of information, in *Philosophy of Information* (*Handbook of the Philosophy of Science*), eds. P. Adriaans and J. van Benthem, Ch. 5b (North Holland, Amsterdam, 2008), (also arXiv:0708.2837v2).
[2] R. Landauer, The physical nature of information, *Phys. Lett. A* **217** (1996) 188–193.
[3] J. Gea-Banacloche and L. B. Kish, Comparison of energy requirements for classical and quantum information processing, *Fluct. Noise Lett.* **3** (2003) C3–C7.
[4] P. C. W. Davies, The implications of a cosmological information bound for complexity, quantum information and the nature of physical law, *Fluct. Noise Lett.* **7** (2007) C37–C50.
[5] L. B. Kish, G. P. Harmer and D. Abbott, Information transfer rate of neurons: Stochastic resonance of Shannon's information channel capacity, *Fluct. Noise Lett.* **1** (2001) L13–L19.
[6] M. J. Berryman, A. Allison and D. Abbott, Mutual information for examining correlations in DNA, *Fluct. Noise Lett.* **4** (2004) L237–L246.
[7] S. Gabarda and G. Cristóbal, Generalized Rényi image entropy: A new noise measure, *Fluct. Noise Lett.* **7** (2007) L391–L396.
[8] F. Chapeau-Blondeau, D. Gindre, R. Barillé and D. Rousseau, Optical coherence of a scalar wave influenced by first-order and second-order statistics of its random phase, *Fluct. Noise Lett.* **8** (2008) L95–L111.
[9] A. Delahaies, F. Chapeau-Blondeau, D. Rousseau and F. Franconi, Tuning the noise in magnetic resonance imaging to maximize nonlinear information transmission, *Fluct. Noise Lett.* **12** (2013) 1350005, 1–16.

[10] A. K. Surridge, D. Osorio and N. Y. Mundy, Evolution and selection of trichromatic vision in primates, *Trends Ecol. Evolution* **18** (2003) 198–205.
[11] G. H. Jacobs, Evolution of colour vision in mammals, *Philos. Trans. Roy. Soc. B* **364** (2009) 2957–2967.
[12] C. E. Shannon, A mathematical theory of communication, *Bell Syst. Techni. J.* **27** (1948) 379–423, 623–656.
[13] T. M. Cover and J. A. Thomas, *Elements of Information Theory* (Wiley, New York, 1991).
[14] D. H. Foster, K. Amano and S. M. C. Nascimento, Information limits on neural identification of colored surfaces in natural scenes, *Visual Neurosci.* **21** (2004) 331–336.
[15] D. H. Foster, I. Marín-Franch, K. Amano and S. M. C. Nascimento, Approaching ideal observer efficiency in using color to retrieve information from natural scenes, *J. Opt. Soc. Am. A* **26** (2009) B14–B24.
[16] I. Marín-Franch and D. H. Foster, Estimating information from image colors: An application to digital cameras and natural scenes, *IEEE Trans. Pattern Anal. Mach. Intell.* **35** (2013) 78–91.
[17] S. Le Moan, A. Mansouri, Y. Voisin and J. Y. Hardeberg, A constrained band selection method based on information measures for spectral image color visualization, *IEEE Trans. Geosci. Remote Sens.* **49** (2011) 5104–5115.
[18] S. Prasad, Information capacity of a seeing-limited imaging system, *Opt. Commun.* **177** (2000) 119–134.
[19] B. R. Frieden, Restoring with maximum likelihood and maximum entropy, *J. Opt. Soc. Am.* **62** (1972) 511–518.
[20] B. R. Frieden, Maximum-information data processing: Application to optical signals, *J. Opt. Soc. Am.* **71** (1981) 294–303.
[21] N. Bara and K. Murata, Maximum entropy image reconstruction from projections, *Opt. Commun.* **38** (1981) 91–95.
[22] C. Oh and B. R. Frieden, Restoration of a Poisson distributed image using a principle of extreme physical information, *Opt. Commun.* **282** (2009) 2489–2494.
[23] B. E. A. Saleh and M. C. Teich, *Fundamentals of Photonics* (Wiley, New York, 1991).
[24] G. Buchsbaum and A. Gottschalk, Trichromacy, opponent colours coding and optimum colour information transmission in the retina, *Proc. Roy. Soc. Lond. B* **220** (1983) 89–113.
[25] J. J. Atick, Z. Li and A. N. Redlich, Understanding retinal color coding from first principles, *Neural Comput.* **4** (1992) 449–572.
[26] M. H. Brill and T. Benzschawel, Remarks on signal-processing explanations of the trichromacy of vision, *J. Opt. Soc. Am. A* **10** (1985) 1794–1796.
[27] C. C. Chiao, T. W. Cronin and D. Osorio, Color signals in natural scenes: Characteristics of reflectance spectra and effects of natural illuminants, *J. Opt. Soc. Am. A* **17** (2000) 218–224.
[28] H. Horiguchi, J. Winawer, R. F. Dougherty and B. A. Wandell, Human trichromacy revisited, *Proc. Nat. Acad. Sci. USA* **110** (2013) E260–E269.
[29] Y. Murakami, T. Obi, M. Yamaguchi, N. Ohyama and Y. Komiya, Spectral reflectance estimation from multi-band image using color chart, *Opt. Commun.* **188** (2001) 47–54.
[30] J. Hernández-Andrés, J. I. Nieves, E. M. Valero and J. Romero, Spectral-daylight recovery by use of only a few sensors, *J. Opt. Soc. Am. A* **21** (2004) 13–23.
[31] V. Cheung, S. Westland, C. Li, J. Hardeberg and D. Connah, Characterization of trichromatic color cameras by using a new multispectral imaging technique, *J. Opt. Soc. Am. A* **22** (2005) 1231–1240.

[32] G. Sharma (ed.), *Digital Color Imaging Handbook* (CRC Press, Boca Raton, 2003).
[33] S. Delalieux, A. Auwerkerken, W. Verstraeten, B. Somers, R. Valcke, J. K. S. Lhermitte and P. Coppin, Hyperspectral reflectance and fluorescence imaging to detect scab induced stress in apple leaves, *Remote Sens.* **1** (2009) 858–874.
[34] E. Belin, D. Rousseau, T. Boureau and V. Caffier, Thermography versus chlorophyll fluorescence imaging for detection and quantification of apple scab, *Comput. Electron. Agriculture* **90** (2013) 159–163.
[35] W. H. Press, S. A. Teukolsky, W. T. Vetterling and B. P. Flannery, *Numerical Recipes in C++: The Art of Scientific Computing* (Cambridge University Press, Cambridge, 2002).
[36] F. S. Acton, *Numerical Methods That Work* (Mathematical Association of America, Washington, 1990).
[37] S. Pralgauskaite, V. Palenskis, J. Matukas, J. Petrulis and G. Kurilcik, Noise characteristics and reliability of light emitting diodes based on nitrides, *Fluct. Noise Lett.* **7** (2007) L367–L378.
[38] V. Palenskis, J. Matukas, S. Pralgauskaite and B. Saulys, A detail analysis of electrical and optical fluctuations of green light-emitting diodes by correlation method, *Fluct. Noise Lett.* **9** (2010) 179–192.
[39] L. M. Dale, A. Thewis, C. Boudry, I. Rotar, P. Dardenne, V. Baeten and J. A. Fernández Pierna, Hyperspectral imaging applications in agriculture and agro-food product quality and safety control: A review, *Appl. Spectros. Rev.* **48** (2013) 142–159.
[40] D. Lorente, N. Aleixos, J. Gómez-Sanchis, S. Cubero, O. L. García-Navarrete and J. Blasco, Recent advances and applications of hyperspectral imaging for fruit and vegetable quality assessment, *Food Bioprocess Technol.* **5** (2012) 1121–1142.
[41] A. K. Mahlein, U. Steiner, C. Hillnhütter, H. W. Dehne and E. C. Oerke, Hyperspectral imaging for small-scale analysis of symptoms caused by different sugar beet diseases, *Plant Meth.* **8**(3) (2012) 1–13.
[42] J. Qin, T. F. Burks, M. A. Ritenour and W. G. Bonn, Detection of citrus canker using hyperspectral reflectance imaging with spectral information divergence, *J. Food Eng.* **93** (2009) 183–191.
[43] C.-I. Chang, An information-theoretic approach to spectral variability, similarity, and discrimination for hyperspectral image analysis, *IEEE Trans. Inform. Theory* **46** (2000) 1927–1932.
[44] F. Chapeau-Blondeau, D. Rousseau and A. Delahaies, Rényi entropy measure of noise-aided information transmission in a binary channel, *Phys. Rev. E* **81** (2010) 051112, 1–10.
[45] F. Chapeau-Blondeau, A. Delahaies and D. Rousseau, Tsallis entropy measure of noise-aided information transmission in a binary channel, *Phys. Lett. A* **375** (2011) 2211–2219.